

An Algorithm Architecture for Radio Interferometric Data Processing

S. BHATNAGAR,¹ U. RAU,¹ M. HSIEH,¹ J. KERN,² AND R. XUE²

¹National Radio Astronomy Observatory, PO Box O, 1003 Lopezville Rd, Socorro, NM 87801, USA

²National Radio Astronomy Observatory, 520 Edgemont Rd, Charlottesville, VA 22903, USA

(Received June 24, 2025; Revised Aug. 08, 2025; Accepted Aug. 19, 2025)

ABSTRACT

We present a foundational, scalable algorithm architecture for processing data from aperture synthesis radio telescopes. The analysis leading to the architecture is rooted in the theory of aperture synthesis, signal processing and numerical optimization keeping it scalable for variations in computing load, algorithmic complexity, and accommodate the continuing evolution of algorithms. It also adheres to scientific software design principles and use of modern performance engineering techniques providing a stable foundation for long-term scalability, performance, and development cost.

We first show that algorithms for both calibration and imaging algorithms share a common mathematical foundation and can be expressed as numerical optimization problems. We then decompose the resulting mathematical framework into fundamental conceptual architectural components, and assemble calibration and imaging algorithms from these foundational components.

For a physical architectural view, we used a library of algorithms implemented in the LibRA software for the various architectural components, and used the Kokkos framework in the compute-intensive components for performance portable implementation. This was deployed on hardware ranging from desktop-class computers to multiple super-computer class high-performance computing (HPC) and high-throughput computing (HTC) platforms with a variety of CPU and GPU architectures, and job schedulers (HTCondor and Slurm).

As a test, we imaged archival data from the NSF's Karl G. Jansky Very Large Array (VLA) telescope in the A-array configuration for the Hubble Ultra Deep Field. Using over 100 GPUs we achieve a processing rate of ~ 2 Terabyte per hour to make one of the deepest images in the 2 – 4 GHz band with an RMS noise of $\sim 1 \mu\text{Jy/beam}$.

Keywords: Methods: data analysis – Techniques: interferometry – image processing – scientific software

1. INTRODUCTION

Indirect imaging devices, like an aperture synthesis radio telescope, record the data in the Fourier domain, and the raw data needs to be Fourier transformed to convert it into an image. These devices sample the Fourier domain incompletely and irregularly, and the data is corrupted by the troposphere and ionospheric layers of the Earth's atmosphere, and by the chain of imperfect electronic components used in such instruments. Noise-limited imaging with such telescopes requires computationally- and I/O-intensive algorithms to mitigate artifacts arising from incomplete and irregular sampling, the presence of radio frequency interference, and from dis-

tortions introduced by atmospheric effects and instrumental imperfections.

To achieve the scientific requirements of high sensitivity and angular resolution, modern aperture synthesis radio telescopes utilize wide-band receivers on hundreds to thousands of antenna elements spread across distances exceeding 1000 kilometers (e.g. see R. J. Selina et al. 2018). The sky brightness distribution, especially at low radio frequencies, is also stronger and more wide-spread, requiring imaging over wider field of view which further increases the data volume and computing load. The resulting data rates and estimated size of computing for typical imaging experiments with such telescopes are on the order of 100 terabyte per hour, and tens of peta floating-point operations per second (PFLOP/s) (S. Bhatnagar et al. 2021), respectively. Achieving this level of performance necessitates the use of parallel computing across thousands of Execution Points (EPs), where each EP is

Corresponding author: S. Bhatnagar
sbhatnag@nrao.edu

Email: sbhatnag@nrao.edu, urvashi@nrao.edu, mhsieh@nrao.edu, jkern@nrao.edu, rxue@nrao.edu

defined as a “compute node” comprising of multi-core CPUs and GPUs. These systems typically rely on heterogeneous computing hardware, incorporating a range of CPU and GPU architectures. Consequently, software designed for such platforms must be both computationally efficient at the EP level and scalable across large, *heterogeneous* computing environments. Imaging with such telescopes therefore fundamentally requires large scale heterogeneous parallel computing. While this has been recognized in the radio astronomy (RA) community for sometime, routine use of the available computing resources has largely remained elusive, even though multiple computing platforms with the requisite computing power are available.

Assessments from the computing industry and the high-performance computing (HPC) community indicate that computing hardware architectures are expected to evolve more rapidly over the coming decade than in previous ones (e.g. see C. E. Leiserson et al. 2020). The resulting gains in runtime performance will primarily benefit computing workflows capable of efficiently parallelizing across multiple scales to exploit heterogeneous collections of massively parallel and multi-core hardware. Consequently, harnessing the full computational potential of future systems requires the development of algorithms that are highly parallelizable and implementations that are performance-portable scaling effectively from intra-node parallelism (e.g., across multi-core CPUs and multiple GPUs within a single EP) to inter-node parallelism (e.g., across thousands of EPs in tightly coupled or distributed computing environments).

In the RA domain, the advent of next-generation high-sensitivity, high-resolution telescopes is expected to drive a corresponding acceleration in the evolution of algorithms. These algorithms must deliver improved imaging performance while being optimized for execution on rapidly evolving, heterogeneous computing architectures, and must be designed to scale efficiently across multiple levels of parallelism. The overall computing landscape comprising of new EP and parallel computing architectures, and new domain algorithms for the future therefore remains unpredictable.

Future-readiness in this rapidly evolving landscape over the life time of the telescopes, and the software stability necessary on even longer time scales for creative research in algorithm development requires an algorithm architecture grounded in foundational principles. This is essential not only for reusability and scalability, but even more critically for enabling the integration of future, generally applicable algorithms (as opposed to bespoke algorithms narrowly tailored to specific use cases). A software system based on such an architecture is expected to scale in an evolving landscape of computing technology, and domain requirements of increasing data volume, complexity, or computational de-

mands, without requiring frequent time-consuming and expensive redesign and re-implementation of the domain code.

In this paper, we first develop a theoretical framework grounded in the fundamental principles of aperture synthesis and signal processing, and demonstrate that existing algorithms for both calibration and imaging can be described as numerical optimization problems and fit in the *same* framework. We then present a component-level decomposition by identifying a set of foundational algorithmic components, and construct a hierarchical Algorithms Architecture based on these elements. In this architecture, core algorithms are composed from foundational components, while higher-level, domain-specific schemes and processing pipelines are systematically constructed from these core algorithms. As an illustrative example, we show that a core set of domain algorithms serving as the fundamental building blocks for advanced data processing workflows can be effectively developed within this architectural framework.

We validate several aspects of the architecture through a concrete example. An accompanying paper presents the physical architectural view and demonstrates the use of modern performance engineering tools to achieve a performance-portable implementation. This implementation is deployable across a wide range of hardware platforms, from laptops and desktop systems to distributed wide-area networks, such as the Open Science Grid (OSG) in the U.S. and super-computing clusters with tightly coupled nodes. We also discuss the design of a software library comprising of reusable modular components, along with their optimization and runtime performance on heterogeneous platforms with a diverse set of CPU and GPU architectures.

2. THEORETICAL FOUNDATION

The measurements made with a radio interferometric array telescope is described with a linear measurement equation (ME) parameterized for the contributions of the sky brightness distribution, the telescope optics and the electronic elements to the total signal. In the description below, we borrow the theoretical formulation from a number of publications (J. P. Hamaker et al. (1996); R. J. Sault et al. (1996), U. Rau et al. (2009), W. H. Press et al. (1992), S. Bhatnagar & T. J. Cornwell (2017)). The analysis here is limited to calibrating the data and imaging the sky radio brightness distribution. The ME can be expressed as

$$V_{ij}^{Obs}(\nu) = M_{ij}^{DI}(\nu) F \left[M_{ij}^{DD}(\vec{s}, \nu) I(\vec{s}, \nu) \right] + n_{ij}(\nu) \quad (1)$$

V_{ij}^{Obs} is the full-polarization data vector, referred to as the *visibilities*, from a single interferometer made with a pair of antennas indexed by subscripts i and j . I represents the full-polarization sky brightness distribution vector in the direction \vec{s} and at frequency ν . M_{ij}^{DI} and M_{ij}^{DD} are the direction independent (super-script *DI*) and the direction depen-

dent (super-script DD) Mueller matrices respectively. These describe the mixing of the elements of the full-polarization vector for the interferometer ij . \mathbf{F} is the Fourier transform operator, n_{ij} represents the measurement noise which has contributions all statistically significant emission not represented by I , Earth's atmosphere and the telescope hardware. The explicit frequency dependence is dropped in the treatment below for notational clarity, except where necessary to show that the architecture covers algorithms that account for frequency dependence (e.g. by treating and aggregating data binned in narrow frequency ranging in a variety of ways). Detailed description of these can be found elsewhere (e.g. see U. Rau et al. (2009) and references therein).

The Mueller matrices are 4×4 matrices which in most cases can be factored into antenna-based 2×2 Jones matrices as

$$\mathbf{M}_{ij}^{DI} = \mathbf{J}_i^{DI} \otimes \mathbf{J}_j^{DI\dagger} \quad (2)$$

$$\mathbf{M}_{ij}^{DD} = \mathbf{J}_i^{DD} \circledast \mathbf{J}_j^{DD\dagger} \quad (3)$$

The symbols \otimes and \circledast represent outer product and outer convolution³ operations respectively. Solvers directly solve for \mathbf{J}_i s, and \mathbf{M}_{ij} are constructed for use in calibration and imaging.

The *unknowns* in Eq. 1 are the elements of the Jones matrices (\mathbf{J}_i , or of \mathbf{M}_{ij} in general) and the sky brightness distribution (I). The primary goal of the calibration process is to solve for \mathbf{M}^{DI} and \mathbf{M}^{DD} to a sufficient accuracy to allow solving for I . Solving for I to a level statistically consistent with n_{ij} is the primary goal of the imaging process. In many real-life use cases these unknowns are further parameterized and the solvers directly solve for these implicit parameters.

The only *known* quantities in Eq. 1 are the observed data (V^{Obs}) and the noise model. The noise term can be described only statistically and it can be shown (and measured) to be normally distributed. Any successful algorithm for calibration and imaging therefore must lead to solutions for \mathbf{M}_{ij} s and I that satisfies Eq. 1 and leaves residuals that are statistically consistent with n_{ij} . That is, the probability distribution of residuals $V^R = V^{Obs} - V^{Mod}$ must be consistent with the distribution of n_{ij} where V^{Mod} is written in terms of the solutions \mathbf{M}_{ij}^{Mod} and I^{Mod} as

$$V_{ij}^{Mod} = \mathbf{M}_{ij}^{DI,Mod} \mathbf{F} \left[\mathbf{M}_{ij}^{DD,Mod}(\vec{s}) I^{Mod}(\vec{s}) \right] \quad (4)$$

The calibration and imaging algorithms can therefore be described as algorithms to estimate n_{ij} for the given V^{Obs}

by appropriately selecting \mathbf{M}_{ij} and I from an otherwise unbounded parameter space. A successful algorithm therefore requires a metric which when minimized (within the bounds of algorithmically determined constraints on the search space), leaves residual consistent with the noise. It can be shown that n_{ij} is normally distributed, for which the weighted χ^2 function is the optimal metric – a standard result of statistical analysis – given by

$$\chi^2 = \sum_{ij} \left[V_{ij}^R \right]_{ij}^\dagger w_{ij} \left[V_{ij}^R \right]_{ij} \quad (5)$$

where w_{ij} are the measurement weights proportional to the inverse of the variance in the measurement noise (n_{ij}).

For runtime scaling, the FFT algorithm is used for the \mathbf{F} operator in Eq. 4, which requires data on a regular grid. V_{ij}^{Mod} however exists only for coordinates determined by the location of the antennas i and j on the ground, which are not on a regular grid. Therefore, in practice a re-sampling operator \mathbf{D} is required to resample the output of the FFT to the coordinates of the sampled data. Here, this operator is parameterized as $\mathbf{D}(c_{ij})$, where c_{ij} is the interpolation kernel used to compute V_{ij}^{Mod} as

$$V_{ij}^{Mod} = \mathbf{M}_{ij}^{DI,Mod} \mathbf{D}(c_{ij}) \mathbf{F} \left[\mathbf{M}_{ij}^{DD,Mod}(\vec{s}) I^{Mod}(\vec{s}) \right] \quad (6)$$

Similarly, the reverse operator $\mathbf{G}(c_{ij})$ is required for resampling the irregularly sampled data (e.g. V^R) on to a regular grid and compute the image using the FFT algorithm for Fourier transform.

$$I^{Mod} = \mathbf{F}^\dagger \sum_{ij} \mathbf{G}(c_{ij}) w_{ij} V_{ij}^R(\vec{u}_{ij}) \quad (7)$$

where \vec{u}_{ij} is the location of the interferometer ij on the spatial frequency plane, and the summation indicates accumulation on a grid at the pixel corresponding to \vec{u}_{ij} . For brevity, V_{ij} is used to indicate measurements at \vec{u}_{ij} in the spatial frequency domain. Symbols \mathbf{D}_{ij} and \mathbf{G}_{ij} are used where c_{ij} varies with i and j , and just \mathbf{D} and \mathbf{G} otherwise. These in the RA literature are also referred to as the “de-gridding” and the “gridding” operators, respectively. The convolutional kernels used in these operators is also explicitly specified as a parameter only where it is necessary for clarity (as in Sec. 6).

The parameter space in which the χ^2 surface is defined can be thought of as a space of calibration and image models (the \mathbf{M}_{ij}^{Mod} and I^{Mod}). Minimizing χ^2 using the derivative to estimate the update direction in this space for iteratively updating the models leads to directed-search algorithms. We show below that most existing algorithms can be described in this framework. For example, we show that for iterative image reconstruction algorithms, the residual image is the update direction, which is used to iteratively update the image model. Similarly, equating to zero the derivative with

³ The element-by-element algebra of the outer-convolution operator is the same as that of the outer-product operator used in the direction-independent (DI) description by J. P. Hamaker et al. (1996), except that the complex multiplications of outer-product are replaced by the convolution operator (S. Bhatnagar et al. 2013).

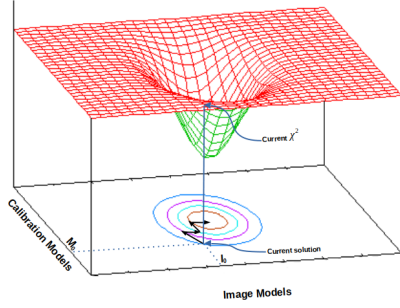


Figure 1. The χ^2 hyper-surface (in red) shown in a space of calibration and image models. The current solution is shown as the point with coordinates (M_o, I_o) , where M_o and I_o represent the starting calibration and image model respectively. The arrows overlayed on the contour plot show successive application of the calibration and imaging solvers to iteratively move the solution to minimize the metric in Eq. 5.

respect to J_i s (or its elements) gives the expressions for the update direction in core calibration algorithms. These algorithms have proved to be both computationally and numerically most competitive and are the most commonly used algorithms. Other variants that differ in how the constraints are imposed to limit the search space are also possible. Non-directed search algorithms (e.g., the family of Monte Carlo-style, or machine learning based algorithms) are also admissible and some are in use. Note that even for such algorithms, goodness-of-fit criteria unsurprisingly involves the use of the χ^2 function, and in many cases even its derivative.

The algorithms for calibration and imaging are iterative in nature. This is also rooted in the numerical analysis theory independent of any domain specific knowledge of the parameters of interest – while the calibration problem is inherently non-linear in antenna-based parameters, imaging process constitutes an ill-posed problem. Successful algorithms use simplifying assumptions that allow treating the phase space as locally orthogonal and iteratively moving the current solution towards the minima in a fundamentally non-orthogonal search space. As a result, while the solvers for I^{Mod} and M^{Mod} are themselves iterative, the solver for the full ME (Eq. 1) in the hyper-space of calibration and image models is also iterative in nature. This is depicted graphically in Fig. 1 for conceptual understanding.

No domain-specific knowledge about the parameters of interest has been used so far. The ME is derived from the basic theory of aperture synthesis, and the conclusions about the solvers are based on the fundamental statistics and signal processing theories. Solvers for a parameterized ME based on this analysis are therefore foundational in nature and would form an important part, if not the basic building blocks of

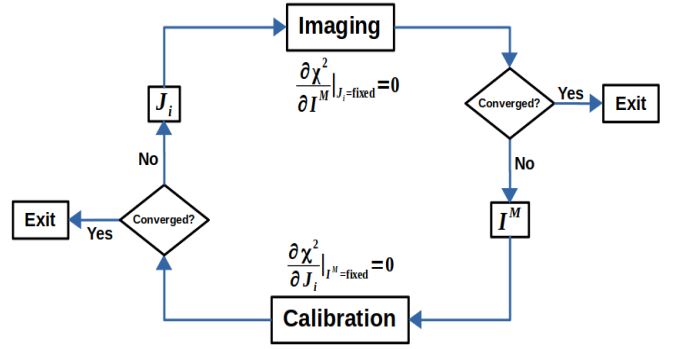


Figure 2. The general structure of an iterative calibration-imaging solver (also known as the *Self Calibration* procedure). As an example of hierarchical algorithm development, Fig. 6 shows such a solver built using the independent calibration and image solvers as architectural components developed in Sec. 5.1 and 5.2 respectively.

useful algorithms and data processing workflows. Architectures based on such a foundational framework will also be extensible – they can accommodate new, general-purpose algorithms that may not yet exist, ensuring long-term adaptability to innovations in domain algorithms, computing software and hardware technology.

In the following sections we give a brief overview of some relevant numerical minimization algorithms and their decomposition into generic fundamental components. We then cast the RA domain core algorithms as function optimization algorithms, which are then assembled with these generic components. Higher level domain algorithms (e.g. the calibration-imaging “SelfCal loop” shown in Fig. 2) and pipelines are assembled from these foundational domain algorithms in a hierarchical algorithms architecture.

3. GENERAL STRUCTURE OF THE CALIBRATION AND IMAGING ALGORITHMS

As mentioned earlier, the unknowns in Eq. 1 are the calibration models M^{DI} and M^{DD} and the sky brightness model $I(\vec{s})$. The M s model the corruptions in the data domain, while I models the sky brightness distribution. Solvers search for optimal models in the hyper-space of calibration and image models by minimizing the χ^2 metric subject to constraints that limit the search space, depicted graphically in Fig. 1.

The coordinates (M_o, I_o) in Fig. 1 indicates the location of the current solution. Ideally, a joint solver that *simultaneously* solves for both models is required to reach the minimum on this surface. While such a solver can be assembled using the basic architectural components derived from numerical optimization considerations as described in Sec. 4.1, the computational and algorithmic complexity of such solvers is significantly higher compared to calibration and image solvers separately. A widely used approach in numerical optimization therefore is to assume that the search

space is *at least* locally orthogonal and devise schemes to approach the minima by the application of calibration or imaging algorithms separately in success steps to move the solution along one of the axis at a time, as shown with arrows overlayed on the contour plot in Fig. 1.

Calibration algorithms are derived by solving the following system of equations, keeping I^{Mod} constant

$$\left. \frac{\partial \chi^2}{\partial \mathbf{J}_i^{Mod}} \right|_{I^{Mod}=constant} = 0 \quad (8)$$

Similarly, imaging algorithms are derived keeping the calibration model \mathbf{M}_{ij}^{Mod} fixed and solving the system of equations given by

$$\left. \frac{\partial \chi^2}{\partial I^{Mod}} \right|_{\mathbf{M}_{ij}^{Mod}=constant} = 0 \quad (9)$$

Solvers for these system of equations are iterative themselves, and can be assembled with specific implementations of components used in numerical optimization as described in sections 4.1 and 5.

A joint solver can be assembled with successive application of these calibration and imaging algorithms as shown in Fig 2. The iterations are bootstrapped, e.g. with a pre-existing image model to derive improved calibration models, which are then used to further improve the image model at each iteration. This general structure is referred to as the Self-Calibration procedure and embodies the assumption of a locally orthogonal phase space.

Higher level, more complex algorithms can thus be built by assembling lower level simpler components in a hierarchical manner. Calibration and imaging algorithms are assembled using foundational components, while a joint solver for the full ME is assembled using calibration and imaging algorithms. Even higher level constructs, e.g. algorithms that partition the image or the data, or both, heuristics for automatic processing pipelines, etc. can be assembled with a mix-and-match of algorithms and even basic components from lower levels of the algorithmic hierarchy.

3.1. Cross domain collaborations

The fundamental conceptual components required for both calibration and imaging are the same – namely, component to (a) compute the derivative of the χ^2 , (b) compute the residual vector for the current model parameters, and (c) update the current parameter values. These steps typically involve some domain knowledge since the models are domain specific by definition, but also because these steps have high computational complexity. For example, calculations of the residuals for calibration involves solving and application of current calibration models to compute nominally corrected data (see Sec. 5.1), while for imaging the derivative compu-

tation involves the expensive data resampling and FFT operations (see Sec. 5.2). Such challenges of overall complexity are common across other domains that rely on numerical optimization, and addressing them will benefit from collaborations with experts from other communities – particularly in high-performance computing and numerical optimization communities. Such cross-domain collaborations to be effective necessitates that the problem formulation is expressed in a shared, standard mathematical language – as against in non-standard domain-specific narrative. Casting RA algorithms in the standard language of numerical optimization therefore offers at least the following benefits:

1. Enables participation by non-RA experts. People from many other fields who are fluent in numerical techniques but may not be familiar with RA jargon can understand the algorithms and be able to contribute effectively.
2. Enables use of well-regarded reliable numerical libraries. This, apart from getting RA community plugged into the larger community of scientific computing professionals, it also opens up the path for experimenting with more sophisticated numerical techniques, implementations of which exists with pluggable components.

The take-away point here is that the structure of both calibration and imaging algorithms is mathematically the same, and can be described in standard terminology. Both type of algorithms are either direct χ^2 -minimization algorithms, or χ^2 minimization forms an integral part of the solver. An hierarchical architecture where domain-specific functionality is built from more basic components, which are themselves described in a standard mathematical language enables effective cross-domain collaborations without the need for the experts from other domains to first fully understand domain specific details.

4. STRUCTURE OF χ^2 MINIMIZATION ALGORITHMS

This section contains an overview of the numerical optimization concepts used in later sections (see standard text books, e.g. W. H. Press et al. (1992), for a more comprehensive description).

Starting from an initial estimate, the parameter vector \vec{P} is updated in the k^{th} iteration as:

$$\vec{P}^{k+1} = \vec{P}^k - \mathbf{H}^{-1} f(\vec{\nabla}_P \chi^2) \quad (10)$$

where \mathbf{H} is the Hessian matrix. Its elements are given by

$$H_{ij} = \frac{\partial^2 \chi^2}{\partial p_i \partial p_j} \quad (11)$$

where p_i are elements of \vec{P} .

Conceptually, $f(\vec{\nabla}_p \chi^2)$ represents the estimated direction towards the minima on the χ^2 -surface along which the parameters are moved, and the elements of \mathbf{H}^{-1} represents the step size. A pure diagonal \mathbf{H} would indicate a strictly orthogonal parameter space, where the update equation simplifies to:

$$P_i^{k+1} = P_i^k - \left[\frac{\partial^2 \chi^2}{\partial P_i^2} \right]^{-1} f\left(\frac{\partial \chi^2}{\partial P_i^k}\right) \quad (12)$$

The residuals, especially closer to the minima, are dominated by noise and the derivative also approaches small values. The $[H_{ii}]^{-1}$ therefore progressively becomes numerically unstable as the iterations proceeds towards convergence. Numerical computation of H_{ii} can also be expensive. To avoid these problems, a commonly used solution in general is to use a fixed step size (e.g. the loop-gain), or an empirically determined value, or a value derived with domain-specific heuristics. Using α as the step size, the update equation is expressed in a familiar form as

$$P_i^{k+1} \approx P_i^k - \alpha f\left(\frac{\partial \chi^2}{\partial P_i^k}\right) \quad (13)$$

Speed of convergence is sometimes improved using H_{ii} when χ^2 is large (indicating the current solution is far from the minima) and a constant closer to the minima. Variants of Eq. 13 used in some other domains are parameterized with heuristics to update the parameters. Eqs. 14 and 15 below show two widely used variants.

Steepest descent + Gauss-Newton:

$$P_i^{k+1} \approx P_i^k - \alpha f\left(\frac{\partial \chi^2}{\partial P_i^k}\right) - \beta \mathbf{h}^{-1} \quad (14)$$

Levenburg-Marquardt (LM):

$$P_i^{k+1} \approx P_i^k - \beta \mathbf{h}'^{-1} \quad (15)$$

where $h'_{ij} = h_{ij}(1 + \delta_{ij}\lambda)$, $h_{ij} = \frac{\partial \chi^2}{\partial p_i} \frac{\partial \chi^2}{\partial p_j}$, and $\delta_{ij} = 1$ for $i = j$ and zero otherwise. Use of Eq. 14 with large α relative to β when the solutions are far from optimal, and increasing the value of β relative to α nearer the minima may improve convergence and even solutions at low SNR. Some schemes switch to Eq. 15 closer to the minima.

Exit criteria to terminate the iterations is often based on domain-specific heuristic derived from the current value of \vec{P} , the χ^2 and $\vec{\nabla}_p \chi^2$, or simply by limiting the maximum number of iterations. For example, one of the criteria used to terminate iterations in image reconstruction is when $\max(\vec{\nabla}_p \chi^2) < \text{threshold}$ is satisfied. Calibration iterations are typically terminated when the change in \vec{P} from one iteration to another

is smaller, or when the χ^2 is smaller than a threshold. In the description below we use $T(\vec{P}, \vec{\nabla}_p \chi^2, \chi^2)$ to encapsulate the termination heuristics.

An architecture for RA algorithms based on this generic formulation would be algorithmically extensible. Current implementations, which are mostly Steepest Descent methods ($\beta = 0$ in Eq. 14), can be easily realized while leaving the option of using other optimization methods (e.g., H. Müller et al. 2025). An architecture build on fundamentals – as against on non-standard domain-specific narrative – can also be a foundational basis for developing new algorithms which may evolve with computing technology.

4.1. Component level decomposition

We decompose the above generic framework into basic, fundamental components required to develop a foundational architecture for a generic solver (Fig. 3). In Sec. 5, RA algorithms are also described as numerical optimization problems, and mapped to the generic solver as specialized architectural views.

Some of the components are foundational in nature derived from fundamental theory (e.g. the `UpdateDir` and `ModelUpdate` components) while some others are derived from the requirements of extensibility, robustness, runtime reliability and computational efficiency. These are also expressed in general conceptual terms at the architectural level (e.g. the `PreSolvePrep` or the `InTransform` components).

1. **UpdateDir:** A component that encapsulates the computation of the update direction – the function f in Eq. 10. In general, this component is applied to all of the data necessary for the required accuracy in the solutions and therefore often drives the overall computational cost.
2. **ModelUpdate:** A component that encapsulates parameter update. Among other domain specific things, this component needs access to the derivative, value of the penalty function (χ^2 with any additional terms, e.g. various forms of algebraic regularization terms), and the current parameter vector.
3. **StepSize:** A sub-component used in the `ModelUpdate` component for the step-size to update the vector of parameters in the direction given by the `UpdateDir` component. Introduction of this architectural component opens the path for more sophisticated approaches that may deliver improved rate of convergence, improved numerical performance, or both.
4. **ExitCriteria:** A component that determines the termination condition for iterative algorithms. Implementations typically rely on a combination of theoretical guidelines and domain-specific heuristics. These

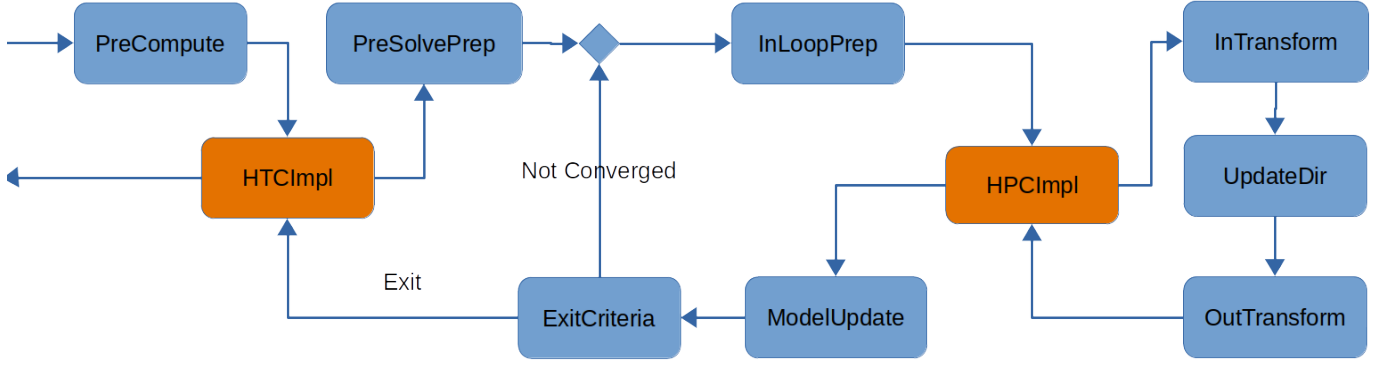


Figure 3. The conceptual architecture for a general solver built with architectural components derived from theoretical analysis. The components for parallelization or data preparation are for optimization and extensibility.

heuristics may require access to the current value of the penalty function, its derivatives, parameter vectors, the number of iterations executed, and other user-defined parameters to ensure robust and reliable termination.

The physics of the instrument and the hardware implementation of it impose some characteristic scales of coherence on the variations of the model parameters (e.g. instrumental response as a function of frequency and polarization, antenna and dish design, and the signal path through the chain of electronic components, etc.). The parameters may vary at a statistically significant level only at scales larger than these fundamental scales, and are stable at shorter scales. It is therefore often both computationally and numerically advantageous to average the data on these scales. The data may also be transformed, or normalized for improved numerical performance. There may be other operations on the data, e.g., data pre-conditioning, flagging, selection of only the pertinent data, etc. Abstracting these kind of operations away from the fundamental theoretical blocks increases the re-usability and scalability. We therefore introduce the following components in the architecture:

5. **PreCompute**: A component for caching computations that remain fixed for the life cycle of the solver but require access to the full data. For example, shaping the telescope Point Spread Function by data reweighing, or caching the kernels used in the G and D sub-components of the `UpdateDir` component (see Figure 5, Section 5.2).
6. **PreSolvePrep**: A component responsible for data preparation and curation tasks that are independent of the iterations and may be done in parallel on portions of the full data. Typical operations include averaging data along various axes, especially where such pre-processing is required prior to the application of the solvers for antenna-based parameters (e.g., see Eq.19 of Sec.5.1). The placement of this component within

the overall framework may vary depending on the specific use case.

7. **InLoopPrep**: A component for iteration-dependent data transformation and curation operations (e.g. use of data flagging information discovered during iterations).

In certain imaging use cases, the same input data contributes to different outputs (for example, in multi-term multi-frequency synthesis (MT-MFS) (U. Rau & T. J. Cornwell 2011)). Similarly, there are scenarios where multiple outputs are generated from input data that has undergone complex transformations, and these intermediate outputs are subsequently combined in non-trivial ways to construct the final desired output. Examples of such use cases include multi-field imaging, image-plane mosaicking (G. B. Taylor et al. 1999), and wide-field imaging algorithms such as faceting and the W-projection/W-snapshot methods (T. J. Cornwell & R. A. Perley 1992; T. J. Cornwell et al. 2012). To cover such use-cases we introduce the following transform components at the input and/or the output of the `UpdateDir` component:

8. **InTransform**: A component that applies transform on the input data stream before it is used for the derivative calculation.
9. **OutTransform**: A component that applies transform, including aggregation, at the output of the `UpdateDir` component.

These components may have a coupling. For example, `OutTransform` component may need to know about the `InTransform` component for mathematical consistency. These components may be at the input and output of the `HPCImpl` component (see Sec. 4.1.1), or be one of the sub-components that together realize the calculations of the derivative in the `UpdateDir` component.

Figure 3 shows a block-level diagram for a generic solver built from these component blocks. In Sec. 5 we map components of RA algorithms to these generic components and show that the architecture delivers the existing algorithms, and is extensible for new algorithms in the future.

4.1.1. A comment on parallelization

There are two components in the block diagram in Fig. 3 for parallelization – the `HTCImpl` and the `HPCImpl` components – each of which are envisioned to serve a different and a distinct purpose. `HTCImpl` should be thought of as a mechanism for cluster-level parallelization (Same Program Multiple Data (SPMD) paradigm). `HPCImpl` is a lower-level parallelization mechanism and may be considered as targeting node-level, and more specifically, *local*, optimization at the EP level. For example, it enables the utilization of multiple compute units (GPUs, CPUs, FPGAs, etc.), multiple cores across CPUs, partitioned GPUs, and non-trivial coordination between the host CPU and associated GPU resources on a single EP. This provides a framework block for a different class of parallel code that may require hardware-specific implementations to fully exploit local hardware and data proximity. This component may be part of the `UpdateStep` block or placed outside it, depending on the overall runtime optimization strategy. Its location may also be a higher-level packaging or API decision, which can be deferred to a later stage of development.

Put another way, `HTCImpl` represents implementation of High Throughput Computing (HTC) while `HPCImpl` represents implementation of High Performance Computing (HPC). Since multiple definitions exist, to clarify what we mean by these terms, below is the definition we use:

High-throughput computing (HTC) refers to parallel computations where individual tasks do not need to interact at runtime, or require small bits of information exchange. High-performance computing (HPC) on the other hand refers to parallel computations where frequent and rapid exchanges of intermediate results may be required to perform the calculations. HPC codes are based on tightly coupled MPI, OpenMP, GPU, and hybrid programs and require low latency interconnect. In contrast to HPC, which uses a single "supercomputer," HTC distributes tasks over many computers and collecting results at the end of all parallel tasks. For example, computing grids composed of heterogeneous resources (clusters, workstations, etc).

The HTC and HPC definitions describe distinct operations for problems which can be cast in the data-parallel paradigm.

However, it is easy to imagine HPC-type operations included in the `HTCImpl` component, and the other way around. For example, `HTCImpl` may launch multiple data-parallel execution graphs, each with its own `HPCImpl` component. For EPs with multiple CPUs and GPUs, this `HPCImpl` component may include HTC-type operations cognizant of data locality and high bandwidth inter-connection at the EP to further manage the partitioning of the quantum of the data at each EP and optimize the workflow for multiple CPU-GPU combination. It is therefore useful to have `HTCImpl` and `HPCImpl` as distinct architectural components with the understanding that they may share parallelization techniques and tool-chain.

5. ARCHITECTURAL VIEWS

Figure 3 shows a view of the conceptual architecture for a generalized solver build with the architectural components identified in the previous sections. In this section we show different views of this generalized architecture for a variety of solvers for calibration and imaging models with specialization of the various components, some of which are further decomposed into sub-components for re-usability.

We use existing algorithms as case studies to show that the architecture is foundational in nature. These core set of algorithms form the building blocks of an hierarchical domain algorithmic architecture. A comprehensive coverage of *all* RA algorithms in use is however out of scope for this paper. Not all direction-dependent techniques in use are therefore covered here (e.g., T. J. Cornwell & R. A. Perley (1992); T. J. Cornwell et al. (2012); U. Rau et al. (2019)). While the architectural framework developed here is designed to accommodate these and other similar methods, further work is necessary to cast and verify those algorithms in this framework.

5.1. Architectural View for Calibration

For clarity here we discuss a direction-independent solver for only the diagonal elements of the Jones matrix (the *G*-Jones solver) and frequency (the *B*-Jones solver). A solver for *D*-Jones (off-diagonal elements of the Jones matrix), or a full-Jones solver can be similarly developed (see e.g., S. Bhatnagar & T. J. Cornwell (2017)).

The multiplicative gains per interferometer can be expressed as an outer product of two 2×2 Jones matrices, one for each antenna of the interferometer. The observed data is the modeled as

$$\vec{V}_{ij}^{obs} = [\mathbf{J}_i \otimes \mathbf{J}_j^\dagger] \vec{V}_{ij}^{Mod} + n_{ij} \quad (16)$$

The diagonal elements of the Jones matrix represent the complex gain for the signal from the two nominally orthogonally polarized receivers, while the off-diagonal elements represent the leakage of signals from one receiver into another. In terms of the equivalent Mueller matrix, the corrected data \vec{V}^c

is expressed as:

$$\vec{V}^c = M_{ij}^{-1} \vec{V}^{Obs} \quad (17)$$

In general, the overall Mueller matrix is separated into a product of a series of Mueller matrices, each modeling a different part of the signal chain. The precise sequences of these matrices is determined by the signal path and in general the product is non-commutative. As a result, in general, effects of the matrices on the left of the Mueller matrix in the ME being solved must be first corrected for (see [CASA Calibration Fundamentals](#)⁴ document for more detailed description). Equation 17 is this application of calibration terms before solving for the elements of the Jones matrix of interest.

In the following description, the multiplicative antenna-based complex gain is denoted by g^p for polarization p , and the super-script pp represents interferometer based parallel-hand products. V^{Mod} represents the (fixed) true expected visibilities. Solving Eq. 8 with this involves first normalizing \vec{V}^c by the model data \vec{V}^{Mod} to increase the signal coherence length and averaging the data for the solution intervals ΔT_{sol} and $\Delta \nu_{sol}$ along time and frequency axis respectively as

$$\vec{V}^{Mod} = DF \vec{I}^{Mod} \quad (18)$$

$$\vec{X}_{ij} = \sum_t \sum_\nu \vec{V}_{ij}^c(t, \nu) [\vec{V}_{ij}^{Mod}(t, \nu)]^{-1} \quad (19)$$

and the χ^2 for a single polarization is then expressed in terms of X_{ij} as

$$\chi^2 = \sum_{ij} \vec{R}_{ij}^{pp*} [W_{ij}] \vec{R}_{ij}^{pp}$$

where $\vec{R}_{ij}^{pp} = \vec{X}_{ij}^{pp} - g_i^p g_j^{p*}$ and $[W_{ij}]$ is the weight matrix.

Equating the derivative $\partial \chi^2 / \partial g_i^p$ to zero leads to a recursive closed-form solution for g_i^p at iteration k , expressed as:

$$\nabla g_i^{p^k} = \frac{\sum_{j,j \neq i} g_j^{p^k} X_{ij}^{pp} w_{ij}^{pp}}{\sum_{j,j \neq i} |g_j^{p^k}|^2 w_{ij}^{pp}} \quad (20)$$

$$g_i^{p^{k+1}} = (1 - \alpha) g_i^{p^k} + \alpha \nabla g_i^{p^{k+1}} \quad (21)$$

α here plays the role of the update step size and balances the contribution of the current solution and the current $\nabla g_i^{p^k}$. The constraint $|\vec{g}^{p^{k+1}} - \vec{g}^{p^k}| < \delta$ is used for the termination criteria where δ is the tolerance limit on the incremental change in the solutions consistent with the estimated antenna sensitivity.

5.1.1. Component level mapping

The above steps map on to the generic components described in Sec. 4.1 and Fig. 3 as follows.

- Equations 17 and 18 map on to the PreCompute component. For DI solver, these are a one-time computation and not dependent on iterations. This is the model prediction and data correction operation which in general requires the D and the F operators, which map on to the re-usable sub-components Degrid and FFT discussed in Sec. 5.2 and shown in Fig. 5. Simpler implementations for model prediction and correction are possible for special cases.
- Equation 19 maps on to the PreSolvePrep component. The summations over time and frequency can be done independently allowing partitioning of the input data. The solver can also be applied on each chunk of data in parallel for the solutions in time and frequency on coherence scales of ΔT_{sol} and $\Delta \nu_{sol}$. This algorithm-level parallelization is achieved via dispatch from the HTCImpl component, or done internally in the component.
- The InLoopPrep component may be a NoOp, or may include heuristics or algorithms, for example, for detection and rejection of poor solutions and data.
- Eq. 20 maps on to the UpdatedDir component. This may also benefit from multi-threaded parallelization at the EP (e.g., by using all available CPU cores at each EP in the HPCImpl component).
- Eq. 21 maps on to the ModelUpdate component.
- Finally, the constraint $|\vec{g}^{p^{k+1}} - \vec{g}^{p^k}| < \delta$ maps on to the ExitCriteria component.

Note that implementations that require numerical evaluation of the derivative – e.g. where closed-form equation is not possible or practical – are also possible. Finally, for terms where transformation and averaging of the data as in Eq. 19 is not possible, the *current* solution may be used in the InLoopPrep component to compute the residual vector (\vec{R}_{ij}) along with related modifications in the PreSolvePrep, UpdatedDir and ModelUpdate components.

5.2. Architectural View for Imaging

Equation 5 for imaging can be expressed as:

$$\chi^2 = [V^C - DF I_k^{Mod}]^\dagger W [V^C - DF I_k^{Mod}] \quad (22)$$

where W is the weights matrix, and subscript k represents the iteration number. With some simple calculus and algebraic

⁴ <https://casadocs.readthedocs.io/en/stable/notebooks/casa-fundamentals.html>

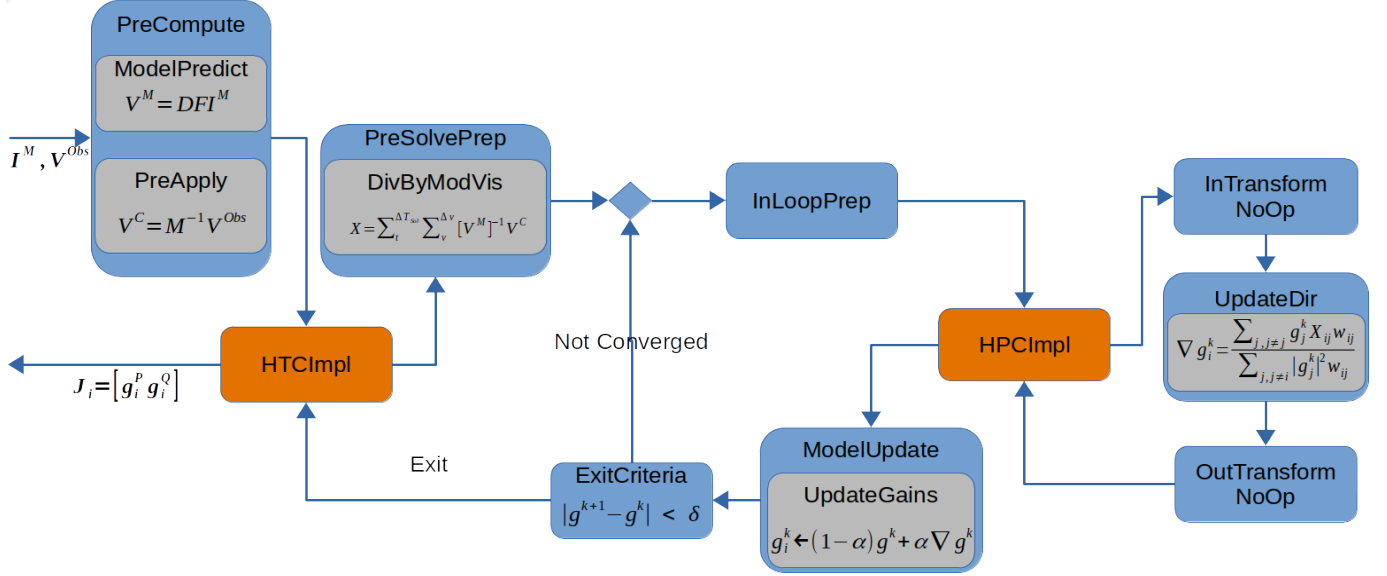


Figure 4. A specialization of the Generic Solver of Fig. 3 for a simple diagonal G-Jones solver. A different specialization of the components shown in gray would deliver solvers for other calibration terms. Inputs are the model image (I^M) and the uncalibrated data (V^{Obs}). Output is the diagonal elements of the Jones matrix (super-scripts P and Q represent the two orthogonal polarizations).

manipulations, it can be shown that $\frac{\partial \chi^2}{\partial I_k^{Mod}} \propto I_k^R$ and

$$I_k^R = \sum_t \sum_\nu \sum_{ij} \mathbf{F}^\dagger \mathbf{G}_{ij} \mathbf{W}_{ij} \left[V^C(t, \nu) - V_k^{Mod}(t, \nu)_k \right]_{ij} \quad (23)$$

The interpretation of the summations over t and v may change depending on the type of imaging modality (continuum, spectral cube, multi-term imaging, or snapshot/temporal movie, etc.). For example, the summation over v for continuum imaging would be an accumulation on to a single image, while for spectral cube imaging it maps individual image(s) on to plane(s) of an image cube. As in the case of the calibration solver, the summations can be done independently, and each can be further partitioned depending on the computer resources.

The model update step of numerical optimization goes by the term “Minor Cycle” in the RA literature. It is itself iterative in nature, and encapsulated here as

$$I_{k+1}^{Mod} = \text{ModelUpdate}\left(\frac{\partial \chi^2}{\partial I^{Mod}}, I_k^{Mod}\right) \quad (24)$$

The algorithms used for `ModelUpdate` range from simple ones that model the sky brightness distribution as a collection of delta functions (e.g. J. A. Högbom (1974)), to complex ones that also account for variations along time, frequency and polarization axis in a scale-sensitive manner (e.g. MS-Clean, MSMFS, Asp-Clean). Details of these algorithms can be found elsewhere in the literature (e.g., see [CASA Imaging Fundamentals](#)⁵, T. J. Cornwell (2008), U. Rau &

T. J. Cornwell (2011), M. Hsieh & S. Bhatnagar (2021)). Mathematically, a modification of Eq. 23 with a straightforward application of the derivative chain rule to compute the update direction for hidden parameters and using them in the `ModelUpdate` component covers these algorithms in the same architectural framework.

The iteration termination criteria is typically a complex heuristic involving the derivative (I_k^R), current model (I_k^{Mod}), number of iterations done (N_{iter}), and mechanisms for forced termination. We encapsulate this in a function as

$$\text{ExitCriteria} = T(I_k^R, I_k^{Mod}, N_{iter}) \quad (25)$$

The derivative computation in general is the most expensive step in most numerical optimization problems. For imaging the computational cost of the G and D operators scale with the total number of independent data points N_{vis} as $\mathcal{O}(N_{vis} \times C_{Sup})$, where C_{Sup} is the support size of the interpolation kernels in number of pixels on the visibility grid. In an end-to-end processing this step may dominate the overall computing cost. The `HPCImp1` component for imaging is therefore typically more complex and much work has been done in the community in general for making the calculations for it and the `ModelUpdate` computationally efficient (e.g., S. van der Tol et al. 2018; M. Pokorný 2021; H. Müller & S. Bhatnagar 2025; M. Hsieh et al. 2025).

5.2.1. Component level mapping

The operations described in Sec. 5.2 map on to the blocks in Sec. 4.1, Fig. 3 as follows.

- The PreCompute component in Fig. 5 as a place holder for one-time operations (e.g. caching the cal-

⁵ https://casadocs.readthedocs.io/en/stable/notebooks/synthesis_imaging.html

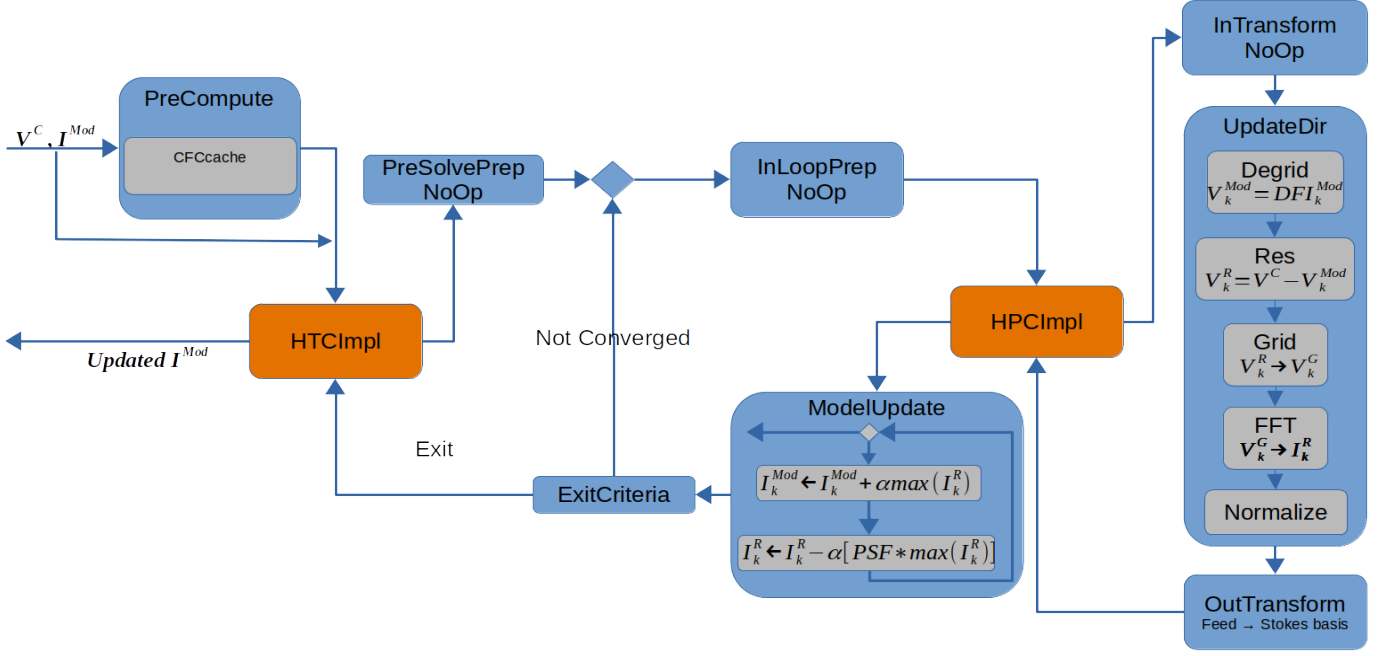


Figure 5. A specialization of the Generic Solver of Fig. 3 for an iterative image solver for single pointing imaging. A different specialization of the ModelUpdate and UpdateDir components would deliver other variants of the solver. The sub-components in gray, especially of the UpdateDir component are re-usable.

- calculations for the convolutional kernels used in the D and G operators).
- Similarly, the PreSolvePrep and InLoopPrep component is a place holder for operations on the quantum of data that flows to the UpdateDir component (e.g. data pre-conditioning, re-ordering for runtime performance benefits, etc.).
- Eq. 23 maps on to the UpdateDir component. This involves several computationally distinct operations shown in Fig. 5 as reusable sub-components. The combined operation of this component is referred to as the “Major Cycle” in RA literature (see CASA Imaging Fundamentals document for more details).
- The summations in Eq. 23 maps on to the OutTransform component. The summations may be implemented as an accumulation (e.g. accumulating the frequency-binned images on a single image for continuum imaging) or a gather operation (e.g. gathering a range of frequency bins on separate planes of an image cube), or a combination thereof.
- Eq. 24 maps on to the ModelUpdate component (referred to as the “Minor Cycle” in the RA literature).
- Eq. 25 maps on to the ExitCriteria component. This may contain sophisticated iteration control heuristics.

- As in calibration, the HTCImpl is responsible for the coarse-gain (algorithm- or cluster-level) parallelization. The implementation of this will depend on the architecture of computing platform and the parallelization strategy used. HPCImpl implements the EP-level parallelization (multi-threading, use of multiple CPUs and GPUs).

6. AN EXAMPLE OF THE PHYSICAL ARCHITECTURAL VIEW

In this section we give an overview of a physical architectural view for imaging, covering a variety of wide-band single pointing and mosaic imaging modalities including some DD corrections (e.g., for the effects of antenna PB, pointing offsets and non co-planar baselines). For this we use the C++ **AWP imaging framework**⁶ from the **LibRA**⁷ project, both of which are described in more detail in the companion paper on physical architecture (S. Bhatnagar et al. 2025). This framework was used to build a highly configurable implementation of the UpdateDir component.

A simplified diagram of the AWP framework is shown in Fig. 7. The framework is parameterized with the VisResampler object which provides services for the G (Gridder) and the D (Degridder) sub-component, a 2D

⁶ <https://safe.nrao.edu/wiki/pub/Software/Algorithms/WebHome/AWPDesign.pdf>

⁷ <https://github.com/ARDG-NRAO/LibRA>

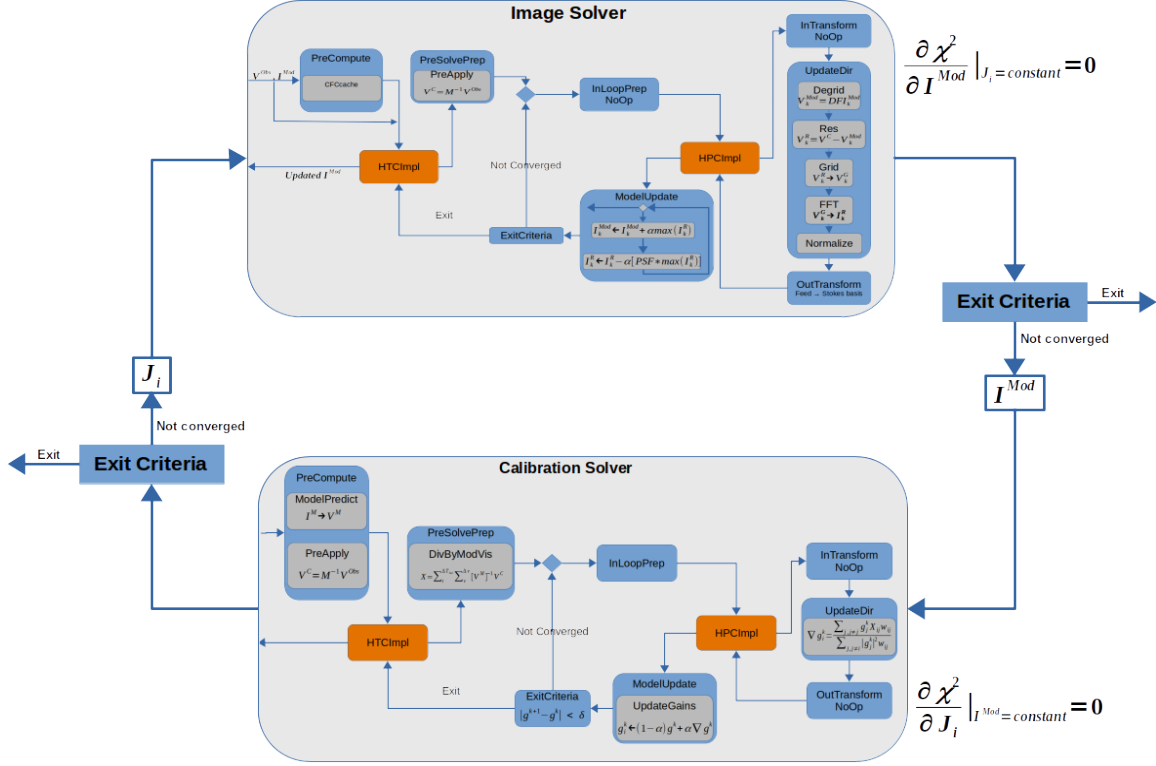


Figure 6. Component level view of the SelfCal concept shown in Fig. 2.

Operation	ATerm	PSTerm	WTerm	CF
AW-Projection	ON	ON OFF	ON ON	PS★A★W A★W
A-Projection	ON	ON OFF	OFF OFF	PS★A A
W-Projection	OFF	ON	ON	PS★W
Standard	OFF	ON	OFF	PS

Table 1. Table of configurations of the AWP imaging framework for a variety of projection algorithms. The symbols A, PS and W represent the A-term, the anti-aliasing Prolate Spheroidal and the W-term functions respectively, and ★ represents the convolution operator.

sparse Mueller matrix of CFs (FM_{ij}^{DD}) used in the G and D operations, and the CFCache plugin component to build and manage a cache of CFs. The sparse matrix of CFs can also be configured to include only terms that are significant compared to the telescope sensitivity. Configuring these plugin components enables a wide range of imaging modalities including single pointing, pointed and on-the-fly mosaic imaging, optionally for full-polarization imaging with corrections for a variety of DD wide-band, wide-field effects.

The CFCache plugin component manages the in-memory and persistent models of the cache of CFs and can itself be configured as shown in Tab. 1. This allows construction of a

variety of DD projection algorithms, including corrections of antenna pointing offsets. The calculations for the CFs in the cache can be triggered in the PreCompute component, with the CFCache plugin configured to pre-compute the cache. It can also be configured to compute the CFs on-demand for cases where it may be efficient to compute CFs recurrently on demand. A combination of these two types of configurations is also possible which allows growing an existing CF cache with usage.

For the general case of wide-band full-polarization mosaic imaging the computations in the UpdateDir component can be expressed as:

$$I^R(P) = \sum_{P,v,w,ij} F^\dagger G(c_{ij}) W_{ij} [V_{ij}(P, v, w) - D(c_{ij}) I^M(P, v)] \quad (26)$$

where P is the array pointing direction towards the part of the sky being imaged. The convolution kernels c_{ij} for the interferometer ij is further parameterized as

$$c_{ij}(P, v, w) = CF_{ij}(v, w, t) f(\Delta \vec{s}_i - \Delta \vec{s}_j) e^{2\pi i [\vec{s}_0 - (\vec{s}(P) + \Delta \vec{s}_i + \Delta \vec{s}_j)]} \quad (27)$$

where CF_{ij} is constructed from ideal kernels and its construction can be configured as shown in Table 1. While CF_{ij} can be independent for each data, in practice a kernel applies to a set of data points. The rest of the terms in Eq. 27 represents the data-dependent perturbations applied on-the-fly. \vec{s}_0 and $\vec{s}(P)$ are the vectors towards the center of the *joint image* and

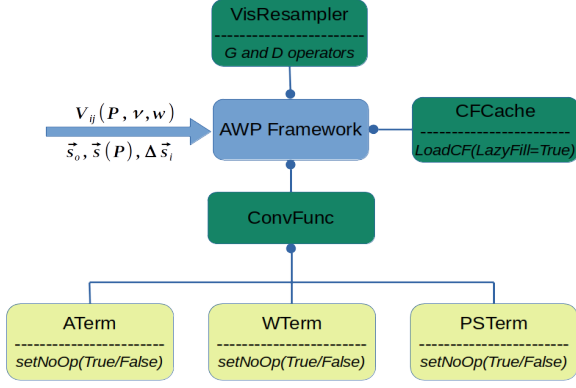


Figure 7. A simplified diagram showing the design of the AWP framework used in Sec. 6 for an example of the physical architectural view. The framework is parameterized with the VisResampler component which implements the re-usable G and D operators, the CFCache component which implements the in-memory and on-disk models for the cache of convolutional kernels c_{ij} , and the ConvFunc component implements the calculations to compute the c_{ij} . The c_{ij} s are further parameterized with the A, W and the PSTerm.

the correlator phase center for pointing P respectively. $\Delta \vec{s}_i$ is the antenna pointing offset for antenna i with respect to the phase center direction $\vec{s}(P)$. f represents any loss in sensitivity due to antenna pointing offsets. It is close to unity for small offsets with $f(0) = 1.0$ and $0 < f <= 1.0$.

\vec{s}_o , $\vec{s}(P)$, and the set of offset vectors $\{\Delta \vec{s}_i\}$ are part of input meta-data for the AWP framework, which enables a number of imaging modalities as tabulated in Table 2.

Imaging mode	Phase center $\vec{s}(P)$	Image center \vec{s}_o	Pointing offset (PO) $\Delta \vec{s}_i$
Single pointing			
No PO correction	\vec{s}_o	\vec{s}_o	0
With PO correction	\vec{s}_o	\vec{s}_o	*
Mosaic imaging			
No PO correction	*	\vec{s}_o	0
With PO correction	*	\vec{s}_o	*

Table 2. Table of configurations for the AWP framework for single or multi-pointing imaging, with or without DD corrections for antenna pointing offsets. * represents value used as-is from the input meta data.

Multi-threaded code to drive the UpdatedDir component and pre-fetch the data and CFs to overlap computing and i/o operations is deployed in the HPCImpl component. The implementation of the VisResampler plugin of the AWP framework in the UpdatedDir component is implemented in the Kokkos framework (H. C. Edwards et al. 2014; C. R. Trott et al. 2022) for performance-portable implementation

of the G and D operators (M. Pokorny 2021). This combination of multi-threaded code on the host CPU and massively-parallel code on the GPU has proven to be scalable, flexible and portable across variety of EP architectures, each with multiple CPUs and GPUs in a single large-scale parallel execution.

A variety of frameworks for data distribution and parallel processing were deployed via the HTCImpl component, ranging from simple Python scripts, generic tools like **gnuparallel**⁸, to functionally more complex and capable schedulers like Slurm and HTCondor. This allowed use of a variety of computing platforms ranging from laptop computers, multi-CPU desktop-class computers and tightly connected clusters, to wide-area distributed clusters and super-computer class machines.

As a test, we used this software system for imaging a few data sets which otherwise would take inordinately long to process. We deployed the UpdatedDir component on the Pathways to Throughput (PATH) computing and the National Research Platform (NRP) computing facilities of the Open Science Grid in the US, utilizing over 100 GPUs of four different architectures in parallel. The PreCompute component was deployed on an in-house cluster using the Slurm scheduler, and the ModelUpdate component was deployed on a single computer with larger memory and faster multi-core CPUs. One of the archived data sets we imaged is from deep integration of the Hubble Ultra Deep Field with the Very Large Array (VLA) in the A-array configuration at S-Band using ~ 2 GHz of the available bandwidth and ~ 100 hr of on-source integration. These parameters require application of the wide-band AW-Projection algorithm (S. Bhatnagar et al. 2013) to correct for the wide-field wide-band instrumental effects and non-coplanarity of the array. The sky brightness distribution at these low frequencies is also stronger and spatially more complex, requiring the use of the MS-Clean algorithm (T. J. Cornwell 2008) to model the sky brightness distribution and mapping a field-of-view covering up to the first sidelobe of the antenna far-field power pattern. Both of these requirements further increases the computing load significantly. As a result, although this data was taken nearly a decade ago, it could not be processed due to excessive run-time and computational costs. With our setup, processing at the rate of ~ 2 Terabyte/hour, convergence was achieved in 10 iterations in about 24 hr of wall-clock run time. The resulting image is one of the deepest image with the VLA with an RMS noise of $\sim 1\mu$ Jy/beam (see **NRAO Newsletter article**⁹, paper in preparation).

⁸ <https://doi.org/10.5281/zenodo.1146013>

⁹ <https://science.nrao.edu/enews/17.3/index.shtml#deepimaging>

6.1. Hierarchical algorithm development

The Self-Calibration procedure for a joint solver, discussed in Sec. 3, is an example of hierarchically building higher level algorithms using lower level components. As shown in Fig. 6 such a joint solver can be built with the image solver described above and a similar calibration solver. The `HTCImpl` component manages the data partitioning and dispatch to EP nodes. For a DI-only calibration solver, operations of the `PreCompute` component may be combined in the `PreSolvePrep` component and executed in parallel. The `HPCImpl` component manages the execution at the EPs of the `UpdateDir` and `ModelUpdate` components. The results are then assembled for the `ExitCriteria` component to determine convergence. Once convergence is achieved, the `PreApply` sub-component of the calibration solver may be used in the `PreSolvePrep` component of the image solver to use data calibrated for the current calibration model. The `ExitCriteria` after the image solver or the calibration may terminate the iterations of this joint solver.

Parallelization is achieved by data partitioning determined by the solution intervals in time and frequency for the calibration solver. Any data reordering for runtime optimization of the solvers is done on-the-fly. With relatively smaller size of the individual data partitions compared to the full data, the runtime overhead of data reordering at the EPs was insignificant.

7. DISCUSSION AND CONCLUSIONS

In this paper we described the algorithms for processing the data from aperture synthesis telescopes in standard terminology of numerical optimization and signal processing. We then developed an algorithmic architecture based on fundamental mathematical concepts, and show that the core algorithms for both calibration and imaging are numerical optimization algorithms which can be expressed in the same architectural framework. In this approach, calibration and imaging algorithms are described as specialized views of the underlying foundational conceptual architecture.

We make two important points. First, that this architecture is built on fundamental concepts and is foundational in nature. Successful algorithms for traditional computer systems (non-quantum computers) – currently or in the future – will require *at least* the architectural components we identify. Algorithms and their implementation based on these components will therefore remain computationally and algorithmically scalable, and adaptable in an evolving overall computing landscape. Secondly, the computing resources required (e.g. memory or FLOP/s footprint) for each of these components may vary significantly. Implementation and optimization of each component can therefore be quite different and may require quite a different tool-chain. It is easy to imagine that the optimal technologies used to harvest the computing

power at various scales may also vary from component to component. The proposed architecture allows modifications, necessitated by changes in the computing environment or in the algorithm used for a given component, to remain confined to that specific component, enabling a modular, mix-and-match approach between components and the hardware on which they are deployed.

Replacing the implementation of a component by a different one is also straightforward, keeping the architecture unchanged. This not only makes the implementation easier to evolve and maintain, but also makes it easier for experts from other domains to contribute to specific parts of the architecture (e.g., use of special hardware for a specific component only). Highly optimized implementation of individual components may even be available from other communities, enabling effective external collaborations. The proposed architecture is inherently scalable, accommodating the continued evolution of hardware, software technologies, and domain-specific algorithms. It also facilitates collaboration with experts from other domains, a capability that is increasingly important in the emerging era of interdisciplinary scientific computing.

As an example, we also present a physical architectural view for an image solver based on the conceptual architecture. For this we use the AWP framework written in C++ for the `UpdateDir` architectural component. This framework is parameterized with plug-in components for the G and D operators, the convolutional kernels used in these operators, and the `CFCache` plugin to manage the in-memory and on-disk models of a cache of these kernels. All of these can be configured in a variety of ways to realize a wide range of algorithms for different imaging modalities. The G and the D operators are themselves implemented in the Kokkos framework (C. R. Trott et al. 2022) for performance portable implementation for use on a variety of massively parallel hardware like GPUs and CPUs with large number of cores (e.g. the ARM architecture). With multi-threading in the `HPCImpl` component for high-performance computing on the host CPU, this design has proved to be flexible and performance-portable and could be easily deployed on a heterogeneous network of remote nodes with a variety of architectures. The `ModelUpdate` component was implemented to enable a range of image-plane modeling algorithms from a library of algorithms from the `LibRA`¹⁰ project (publicly available since 2022), which is a re-engineered fork of the CASA code base (CASA Team et al. 2022). The `HTCImpl` component for high-throughput computing was implemented with a variety of parallelization frameworks on multiple parallel computing platforms rang-

¹⁰ <https://github.com/ARDG-NRAO/LibRA>

ing from multi-CPU desktop-class computers to super computer class distributed and tightly connected clusters.

The configurability of the AWP framework as shown in Tables 1 and 2 allows a wide range of algorithms for the UpdateDir component, while the configurability of the CFCCache plugin allows optimization of the run-time performance and memory management. The ModelUpdate component is independently configured to invoke the algorithms of choice, and it could be optimized independently. In an accompanying paper (S. Bhatnagar et al. 2025), we discuss in more detail the physical architecture with some results and runtime scaling on a few different parallel computing platforms.

The capability to implement the various components quite independently of each other leads to an overall implementation that is efficient and flexible in utilizing a range of available computing platforms. This also enabled effective collaborations with experts from other domains for the various components which together constitute a complex computing stack. For example, the VisResampler plug-in for the AWP framework was developed by in-house experts in collaboration with the Kokkos group and industry R&D groups (M. Pokorny 2021; C. R. Trott et al. 2022). The HTCondor-based implementation of the HTCImpl was developed by in-house experts in collaboration with the staff at the [Center for High Throughput Computing \(CHTC\)](#)¹¹ and the [San Diego Super-computer Center](#)¹². This effectively verifies key architectural goals of efficiency, flexibility and scalability in terms of using computing resource, human expertise, and in enabling a wide range of scientific functionality in an easily configurable implementation.

Here we also note that all this was possible, from conceptualization to deployment and application to real-life problems, due to the effective participation from different, very diverse set of experts from multiple modestly-sized groups,

each with a concentration of expertise in specific parts of the computing stack. Each group could focus on a small part of the architecture without the impractical need of full-system expertise first. This seems to both, reduce the cost and increase the speed of development in an increasingly complex and rapidly evolving overall computing landscape (hardware, software tool-chain, and domain algorithms (C. E. Leiserson et al. 2020)). These considerations are of critical importance for the viability of the next-generation of radio telescopes. These features together also support our conclusion that the mathematical formulation and the resulting architecture described here is foundational in nature. As a future goal, expressing other existing algorithms and new algorithms in this framework without the need for architectural change will independently verify its foundational nature.

ACKNOWLEDGEMENTS

We thank the members of the Algorithms R&D Group of the National Radio Astronomy Observatory (NRAO) for many useful impromptu discussions over the years. We also thank Neeraj Gupta (IUCAA, Pune), George Moellebrock (NRAO, Socorro), Kumar Golap (NRAO, Socorro) and Mark Whitehead (NRAO, Charlottesville) for helpful discussions and the anonymous referee for useful suggestions and corrections. The Very Large Array (VLA) telescope is operated by the NRAO which is a facility of the National Science Foundation operated under cooperative agreement by Associated Universities, Inc.

Software: CASACore (Casacore Team 2019), CASA (CASA Team et al. 2022), LibRA (S. Bhatnagar et al. 2025, <https://github.com/ARDG-NRAO/LibRA>), Kokkos (C. R. Trott et al. 2022), HPG Library (M. Pokorny 2021), WCSLIB (M. R. Calabretta 2011; M. R. Calabretta et al. 2004).

REFERENCES

- Bhatnagar, S., & Cornwell, T. J. 2017, The Astronomical Journal, 154, 197, doi: [10.3847/1538-3881/aa8f43](https://doi.org/10.3847/1538-3881/aa8f43)
- Bhatnagar, S., Hiriart, R., & Pokorny, M. 2021, Size-of-Computing Estimates for ngVLA Synthesis Imaging, Tech. rep., ngEVLA Computing Memo 4.
http://library.nrao.edu/public/memos/ngvla/NGVLAC_04.pdf
- Bhatnagar, S., Hsieh, M., Jagannathan, P., & Madsen, F. 2025, in prep.
- Bhatnagar, S., Rau, U., & Golap, K. 2013, ApJ, 770, 91, doi: [10.1088/0004-637X/770/2/91](https://doi.org/10.1088/0004-637X/770/2/91)
- Calabretta, M. R. 2011, Wcslib and Pgsbox,, Astrophysics Source Code Library, record ascl:1108.003
- Calabretta, M. R., Valdes, F., Greisen, E. W., & Allen, S. L. 2004, in Astronomical Society of the Pacific Conference Series, Vol. 314, Astronomical Data Analysis Software and Systems (ADASS) XIII, ed. F. Ochsenbein, M. G. Allen, & D. Egret, 551
- CASA Team, Bean, B., Bhatnagar, S., et al. 2022, Publications of the Astronomical Society of the Pacific, 134, 114501, doi: [10.1088/1538-3873/ac9642](https://doi.org/10.1088/1538-3873/ac9642)
- Casacore Team. 2019, casacore: Suite of C++ libraries for radio astronomy data processing,, Astrophysics Source Code Library, record ascl:1912.002

¹¹ <https://chte.cs.wisc.edu/>

¹² <https://www.sdsc.edu>

- Cornwell, T. J. 2008, *IEEE Journal of Selected Topics in Signal Processing*, 2, 793–801, doi: [10.1109/jstsp.2008.2006388](https://doi.org/10.1109/jstsp.2008.2006388)
- Cornwell, T. J., & Perley, R. A. 1992, *A&A*, 261, 353.
http://adsabs.harvard.edu/cgi-bin/nph-bib_query?bibcode=1992A%26A...261..353C&db_key=AST
- Cornwell, T. J., Voronkov, M. A., & Humphreys, B. 2012, in *Society of Photo-Optical Instrumentation Engineers (SPIE) Conference Series*, Vol. 8500, *Image Reconstruction from Incomplete Data VII*, ed. P. J. Bones, M. A. Fiddy, & R. P. Millane, 85000L, doi: [10.1117/12.929336](https://doi.org/10.1117/12.929336)
- Edwards, H. C., Trott, C. R., & Sunderland, D. 2014, *Journal of Parallel and Distributed Computing*, 74, 3202 ,
doi: <https://doi.org/10.1016/j.jpdc.2014.07.003>
- Hamaker, J. P., Bregman, J. D., & Sault, R. J. 1996, *A&AS*, 117, 137. http://adsabs.harvard.edu/cgi-bin/nph-bib_query?bibcode=1996A%26AS..117..137H&db_key=AST
- Högbom, J. A. 1974, *A&AS*, 15, 417
- Hsieh, M., & Bhatnagar, S. 2021, Efficient adaptive-scale clean deconvolution in casa for radio interferometric images,
<https://safe.nrao.edu/wiki/pub/Software/Algorithms/WebHome/ardg.aspclean.pdf>
- Hsieh, M., Bhatnagar, S., & Rau, U. 2025, *Astrophysical Journal*, in prep.
- Leiserson, C. E., Thompson, N. C., Emer, J. S., et al. 2020, *Science*, 368, eaam9744, doi: [10.1126/science.aam9744](https://doi.org/10.1126/science.aam9744)
- Müller, H., & Bhatnagar, S. 2025, *Astronomy & Astrophysics*, 698, doi: <https://doi.org/10.1051/0004-6361/202553990>
- Müller, H., Hsieh, M., & Bhatnagar, S. 2025, *Astronomy & Astrophysics*, (submitted)
- Pokorny, M. 2021, High Performance Gridding, Tech. rep., ngEVLA Computing Memo 4.
<https://library.nrao.edu/public/memos/ngvla/NGVLAC.05.pdf>
- Press, W. H., Teukolsky, S. A., Vetterling, W. T., & Flannery, B. P. 1992, *Numerical Recipes in C*, 2nd edn. (Cambridge, USA: Cambridge University Press)
- Rau, U., Bhatnagar, S., Voronkov, M. A., & Cornwell, T. J. 2009, *IEEE Proceedings*, 97, 1472,
doi: [10.1109/JPROC.2009.2014853](https://doi.org/10.1109/JPROC.2009.2014853)
- Rau, U., & Cornwell, T. J. 2011, *A&A*, 532, A71,
doi: [10.1051/0004-6361/201117104](https://doi.org/10.1051/0004-6361/201117104)
- Rau, U., Naik, N., & Braun, T. 2019, *The Astronomical Journal*, 158, 3, doi: [10.3847/1538-3881/ab1aa7](https://doi.org/10.3847/1538-3881/ab1aa7)
- Sault, R. J., Hamaker, J. P., & Bregman, J. D. 1996, *A&AS*, 117, 149. http://adsabs.harvard.edu/cgi-bin/nph-bib_query?bibcode=1996A%26AS..117..149S&db_key=AST
- Selina, R. J., Murphy, E. J., McKinnon, M., et al. 2018, in *Science with a Next-Generation Very Large Array*, ed. E. J. Murphy & the ngVLA Science Advisory Council, *Astronomical Society of the Pacific, Monograph* 7, 15.
https://aspbooks.org/a/volumes/article_details/?paper_id=38661
- Taylor, G. B., Carilli, C. L., & Perley, R. A., eds. 1999, *Synthesis Imaging in Radio Astronomy II*. http://adsabs.harvard.edu/cgi-bin/nph-bib_query?bibcode=1999sira.conf.....T&db_key=AST
- Trott, C. R., Lebrun-Grandié, D., Arndt, D., et al. 2022, *IEEE Transactions on Parallel and Distributed Systems*, 33, 805,
doi: [10.1109/TPDS.2021.3097283](https://doi.org/10.1109/TPDS.2021.3097283)
- van der Tol, S., Veenboer, B., & Offringa, A. R. 2018, *Astronomy & Astrophysics*, 616, A27, doi: [10.1051/0004-6361/201832858](https://doi.org/10.1051/0004-6361/201832858)